

Folding Every Point on a Polygon Boundary to a Point

Nattawut Phetmak and Jittat Fakcharoenphol *

Faculty of Computer Engineering, Kasetsart University, Bangkok 10900, Thailand; nattawut.p@ku.th

* Correspondence: jtf@ku.ac.th

Abstract: We consider a problem in computational origami. Given a piece of paper as a convex polygon P and a point f located within, we fold every point on a boundary of P to f and compute a region that is safe from folding, i.e., the region with no creases. This problem is an extended version of a problem by Akitaya, Ballinger, Demaine, Hull, and Schmidt that only folds corners of the polygon. To find the region, we prove structural properties of intersections of parabola-bounded regions and use them to devise a linear-time algorithm. We also prove a structural result regarding the complexity of the safe region as a variable of the location of point f , i.e., the number of arcs of the safe region can be determined using the straight skeleton of the polygon P .

Keywords: geometric folding; parabola intersection; computational origami; linear-time algorithms; straight skeletons

1. Introduction

Paper folding offers rich computational geometry problems with many real-world applications [1]. The topic, typically referred to as *computational origami* or *mathematics of paper folding* [2,3], studies both feasibility problems and also structural problems [4–6] with the aim to illuminate the connections between physical structures/problems and mathematical geometric objects (see, e.g., [7,8]). As geometric construction using straightedge and compass offers elegant connections between algebra and geometry, paper folding, which can be seen as geometric construction with additional operations, may provide beautiful structural properties worth studying (e.g., see [2,9]).

Akitaya, Ballinger, Demaine, Hull, and Schmidt [4] previously considered two folding problems on a convex piece of paper P . Given a query point p inside P , their first problem, originally proposed by Haga [10–12], called *points to a point*, is to find a region containing p bounded by creases after fold-and-unfold of each corner of P onto p . Their second problem, called *lines to a line*, takes as an input a line ℓ inside P and the goal is to find a region containing ℓ bounded by creases after a fold-and-unfold of each side of P onto ℓ . Although these two problems share a similar structure, they find that the outcomes diverge. That is, the region in the first problem resembles a Voronoi cell [13] with the inner point and corners as seeds, while the region in the second problem relies on the straight skeleton of the piece of paper.

We consider a variant of this folding problem in the same flavor, i.e., we are given a query point f inside P and we are interested in a region containing f bounded by creases after a fold-and-unfold of *every* point on the boundary of the paper δP onto f . We call this result region a *safe region* R since every point $p \in R$ is safe from this folding procedure. Our contributions are an analysis of the shape of R , an efficient algorithm for finding R , and a complexity of the safe region with respect to any query point f .

Figure 1a shows a few creases after folding various points on polygon edge $\overline{v_2v_3}$ onto point f . The resulting safe region is shown in Figure 1b. Figure 2 provides a comparison between point-to-point folding considered in Akitaya et al. [4] (in Figure 2a) and our work (in Figure 2b).



Citation: Phetmak, N.;

Fakcharoenphol, J. Folding Every

Point on a Polygon Boundary to a

Point. *Algorithms* 2023, 16, 281.<https://doi.org/10.3390/a16060281>

Academic Editors: Andreas Kanavos

and Christos Makris

Received: 1 May 2023

Revised: 29 May 2023

Accepted: 29 May 2023

Published: 31 May 2023



Copyright: © 2023 by the authors.

Licensee MDPI, Basel, Switzerland.

This article is an open access article

distributed under the terms and

conditions of the Creative Commons

Attribution (CC BY) license ([https://creativecommons.org/licenses/by/](https://creativecommons.org/licenses/by/4.0/)[https://creativecommons.org/licenses/by/](https://creativecommons.org/licenses/by/4.0/)

4.0/).

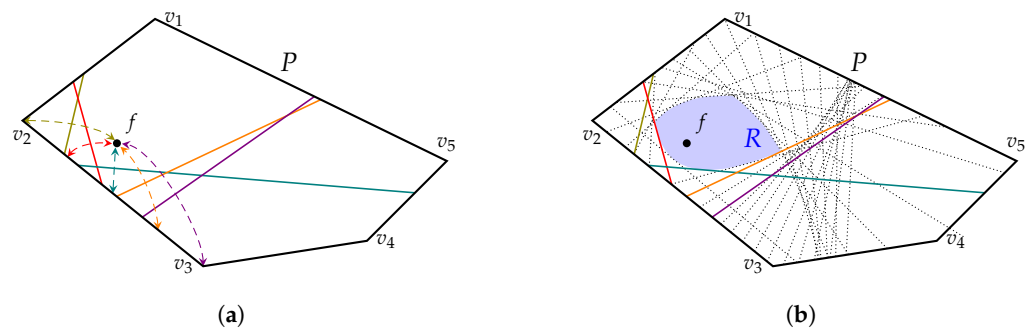


Figure 1. The problem of folding every point on the boundary of a polygon P to a point f . (a) Sample creases from points on edge $\overline{v_2v_3}$; (b) The safe region R .

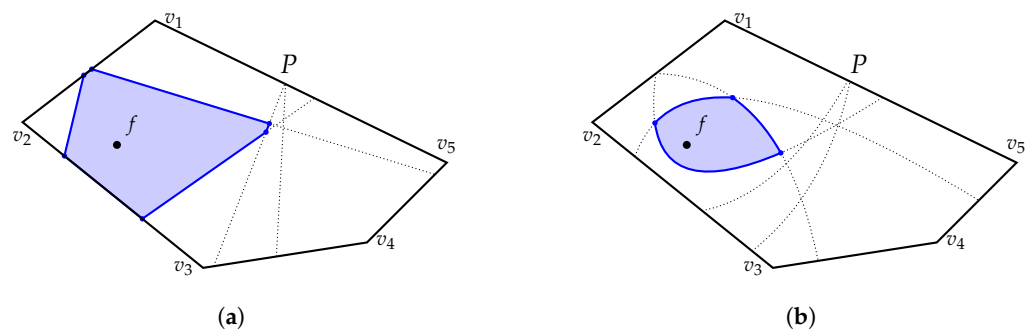


Figure 2. Comparison of the settings of the problem considered in this paper with that of [4]. (a) Corner folding in [4]; (b) Boundary folding in our paper.

We first show that, although we fold infinitely many points on δP , the result region R can be described finitely. It is a well-known result that a fold-and-unfold of multiple points from a line onto a point produces an envelope of a parabola. Thus, we consider each “side” of R as a parabolic arc instead of a traditional straight line segment. The analysis is presented in Section 2.

Using the analysis of the properties of safe regions, we present a linear-time algorithm for finding the region R , given a piece of paper P as a sorted list of n corners in counterclockwise order. Our algorithm works similarly to Graham’s scan for a convex hull. That is, we consider adding one side of P as a parabola arc at a time, maintaining the loop invariant that regulates the region R . During each iteration, we may destroy some of the previously added parabola arcs. The key insight is that the destroyed parabola arc must be the one that is closest to the newly added parabolic region. Thus, it allows us to amortize the cost of destroying, achieving a linear-time algorithm overall. Section 3 explains the algorithm in full detail.

Finally, given any potential query point f , we calculate the precise number of parabola arcs of the region R . They turn out to be dependent on a set of inscribed circles, each of which is centered at a node of the straight skeleton of P . We dedicate Section 4 to focus solely on this property.

We hope that our problem will expand the richness of the family of fold-and-unfold origami problems. Nevertheless, it could serve as a *bridge* joining the previous two problems from [4], since our problem statement is similar to their first problem, but our result is similar to their second problem.

2. Preliminaries

In this section, we provide a formal definition of the problem. We are given a convex polygon P as an ordered list of vertices $V(P) = [v_1, v_2, \dots, v_n]$ in counterclockwise order. We shall treat the list as a circular list. Given two points a and b , we refer to a line segment whose ends are a and b as a segment \overline{ab} . Equivalently, the polygon P is also represented as

a list of edges $E(P) = [e_1, e_2, \dots, e_n]$, where $e_i = \overline{v_i v_{i+1}}$ is a line segment joining v_i and v_{i+1} . We denote its boundary as δP , i.e., $\delta P = \cup E(P)$.

We are also given a point f strictly inside P . Consider a point $u \in \delta P$ on edge $e_i = \overline{v_i v_{i+1}}$. Folding u onto f results in a straight line L , referred to as a *crease line*, which passes through the middle point on the line segment \overline{uf} and is also orthogonal to \overline{uf} . We are interested in the set of crease lines when folding every point on e_i onto f . The envelope of this family of crease lines corresponds to a parabola, whose focus is f and directrix is a line resulting from extending the segment e_i to a line. We refer to this parabola as p_i . See Figure 3.

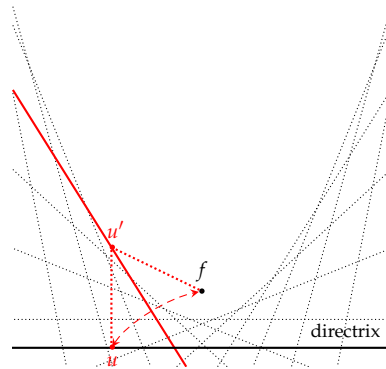


Figure 3. Fold-and-unfold points on a line to a fixed point multiple times, creating an envelope of a parabola.

To see this, let line L' be erected perpendicularly to the directrix at point u , and let $u' = L \cap L'$. We have $|\overline{u'f}| = |\overline{u'u}|$, which indeed obeys the definition of parabolas. In other words, u' is a point on a parabola's curve. Furthermore, for every point $v \in L'$ such that $|\overline{vf}| < |\overline{vu}|$, the point v is "safe" from other creases produced by fold-and-unfold of every other point from this directrix, which is a line extension of the segment e_i .

Since p_i divides the plane into two parabolic half-planes, we are interested in the region containing f . We define a half-space $H(p_i)$ to be the half-plane containing f . More formally, $H(p_i)$ contains all points v such that $|\overline{vf}| \leq |\overline{vu}|$, where u is an orthogonal projection of v on the line extension of e_i .

Our goal is to find:

$$R = \bigcap_{i=1}^n H(p_i),$$

defined to be the *safe region*. When focusing on point f , we sometimes refer to the safe region with respect to point f as R_f .

We describe the algorithm in Section 3. Later in this section, we state relevant geometry facts.

2.1. A Parabola as a Projection of a Conic Section

A parabola can be viewed as a conic section, i.e., a curve on a surface of a cone intersecting a cutting plane tilted at the same angle as the cone. Analytically, we consider a Euclidean space \mathbb{R}^3 . A *cone* is a surface satisfying the equation:

$$x^2 + y^2 - z^2 = 0$$

with an apex of the cone at the origin. A *cutting plane* can be defined with an equation:

$$x \cos \theta + y \sin \theta - z = r,$$

where r is the distance on the xy -plane from the cone’s apex to the nearest point of the cutting plane, and θ is the *directional angle* on the xy -plane to that point. By this definition, we have a parabola as a curve on the tilted cutting plane. See Figure 4a,b.

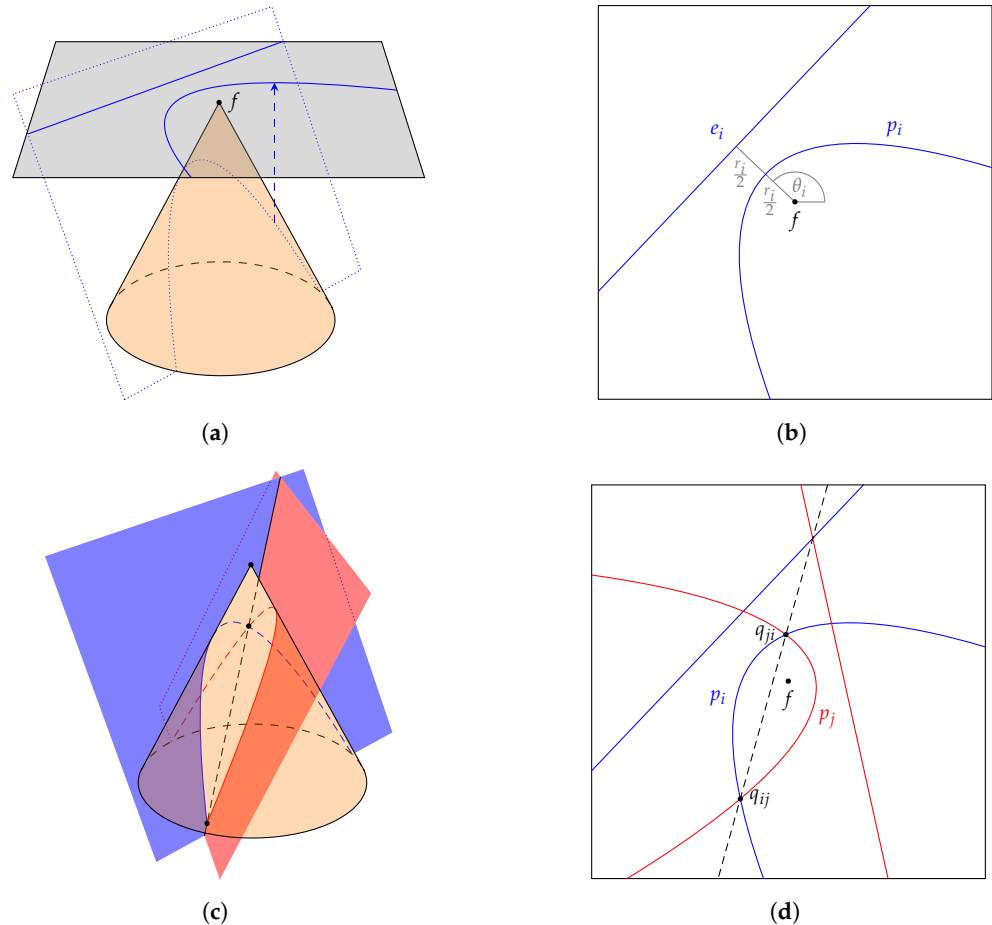


Figure 4. Interpretation of a parabola as a projection of a conic section. (a) Mapping a tilted parabola to the xy -plane; (b) Projection of a parabola on the xy -plane; (c) Two cutting planes; (d) Angle bisector and two intersections.

A projected parabola is an orthogonal projection of the tilted parabola onto the xy -plane, which is also a parabola. The projected parabola has the cone’s apex as its focus, and an intersect line of the cutting plane with the xy -plane as its directrix. This projection viewpoint was briefly mentioned at the end of [14]. In this paper, we refer to projected parabolas simply as parabolas.

We say that parabola p is in the *upright form* if, by rotating and translating the xy -plane, the parabola possesses an analytical form of $y = tx^2$ where $t > 0$.

2.2. Two Parabolas

We define *semi-confocal parabolas* as a family of parabolas that share the same focus, but their directrices do not need to have the same directional angle. It follows that semi-confocal parabolas are projected parabolas from multiple cutting planes that cut the same cone. We state two important facts on intersections of two parabolas which, under the conic interpretation, are straightforward.

Lemma 1. *Two semi-confocal parabolas do not intersect iff their directional angles are the same.*

Proof. Two parabolas with the same directional angle are produced from two parallel cutting planes in the conic view, which never intersect. □

Lemma 2. *If two semi-confocal parabolas intersect, then they intersect at two points which also lie on an angle bisector of their directrices.*

Proof. Take conic section interpretation. Their curves on the surface of the cone must also lie on their cutting planes, in which the intersection of the planes is a straight line. This line piece goes through the cone exactly two times. See Figure 4c,d. □

It follows from Lemma 2 that two intersecting semi-confocal parabolas p_i, p_j produce a safe region $R = H(p_i) \cap H(p_j)$ which is a bounded convex region. Moreover, since we only deal with parabolas whose directrices are from boundary edges of a convex polygon, the non-intersecting case never occurs.

Given two parabolas p_i and p_j , we can compute their intersections using analytical techniques in $O(1)$ time as follows. We reduce the problem of finding intersection of two parabolas to the problem of finding intersection of a parabola and a line. Without loss of generality, we consider p_i in the upright form. From Lemma 2, we find an angle bisector b such that it divides the inner angle between edges e_i and e_j . Then, we find the resulting intersections of p_i and b using quadratic equations.

We remark particularly on the structure of the safe region R .

Consider each parabola p_i in the upright form. We can partition this parabola using the two intersection points into three arcs: the *left arc*, the *central arc*, and the *right arc*, where the left arc corresponds to the half-parabola unbounded to $-\infty$ and the right arc corresponds to the half-parabola unbounded to $+\infty$, and the central arc lies between the two intersection points (see Figure 5). Under this notation, we note that the left arc of p_i intersects p_j only once at the intersection point where it also intersects the right arc of p_j , and vice versa.

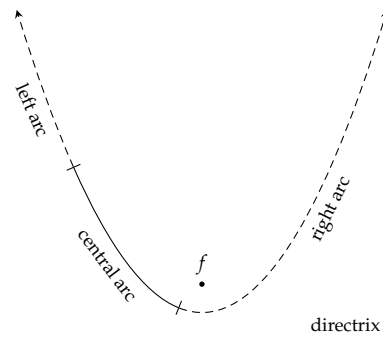


Figure 5. Arc decomposition of a parabola.

In our analysis, where there are parabolas p_1, p_2, \dots, p_n , we refer to the two intersection points between parabolas p_i and p_j as q_{ij} and q_{ji} . To distinguish between these two points, imagine if one traverses counterclockwise on the boundary of $H(p_i) \cap H(p_j)$, then one would see an arc of p_i , the intersecting point q_{ij} , the arc of p_j , and then the intersection point q_{ji} . The counterclockwise definitions of these points are crucial to our proof of Lemma 4. See Figure 4d.

2.3. Many Parabolas

In this section, we analyze the structure of the intersection of k semi-confocal parabolas, extending the result from the previous section.

Let p_1, p_2, \dots, p_k be k semi-confocal parabolas with different directional angles. We shall consider the safe region of these parabolas and prove the following lemma.

Lemma 3. *Each parabola touches at most one arc of the safe region.*

Proof. We prove by induction on k for the case where $k = 2$ follows from Lemma 2. Consider k parabolas. Let $R' = \bigcap_{i=1}^{k-1} H(p_i)$. Inductively, each parabola p_1, p_2, \dots, p_{k-1} touches at most one arc of R' . We consider $R = R' \cap H(p_k)$, we shall show that p_k only touches at most one arc of R . If $R' \subseteq H(p_k)$, then $R = R'$ and p_k does not touch R ; hence, the lemma is true. We then assume that $R' \not\subseteq H(p_k)$.

Clearly, p_k touches one arc of $R = R' \cap H(p_k)$. We call that arc a_k . Each endpoint of a_k belongs to some arc of R' .

There are two cases.

Case 1: Both endpoints of a_k belongs to a single arc of p_i . In this case, p_k intersects exactly one arc of R' exactly twice. Then, the safe region R is the intersection of exactly two parabolas, i.e., $R = H(p_i) \cap H(p_k)$. Thus, the lemma follows from Lemma 2.

Case 2: One endpoint of a_k belongs to p_i while the other belongs to p_j . We show that in this case, p_k intersects exactly two arcs, implying the lemma. We consider p_i first, i.e., we look at the intersection $R_i = H(p_k) \cap H(p_i)$. Let q_i be the intersecting point of p_i and p_k . We can partition p_k into three arcs; let b_k be the unbounded arc starting at q_i . From Lemma 2, we know that b_k only intersects R_i once. Since $R \subseteq R_i$, we have that b_k also intersects R at most once at q_i . We follow the same argument for p_j . Thus, p_k only intersects R' exactly twice, as claimed. \square

3. The Algorithm

Our algorithm for finding a safe region works similarly to Graham's scan [15] for convex hull. We briefly described the algorithm as a pseudocode in Algorithm 1. Later in this section, we explain the algorithm and prove its correctness.

Algorithm 1: Our algorithm for finding the safe region.

```

function SAFEREGION( $P$  : POLYGON,  $f$  : POINT)
   $[e_1, e_2, e_3, \dots, e_n] \leftarrow E(P)$ 
   $p_1 \leftarrow \text{PARABOLA}(f, e_1)$ 
   $p_2 \leftarrow \text{PARABOLA}(f, e_2)$ 
   $q_{12} \leftarrow \text{INNERINTERSECTION}(p_1, p_2)$ 
   $q_{21} \leftarrow \text{INNERINTERSECTION}(p_2, p_1)$ 
   $R \leftarrow \text{DOUBLYLINKEDLIST}(\text{ARC}(p_1, q_{21}, q_{12}), \text{ARC}(p_2, q_{12}, q_{21}))$ 
  for  $i \in [3, 4, 5, \dots, n]$  do
     $p_i \leftarrow \text{PARABOLA}(f, e_i)$ 
     $(p_H, \ell_H, r_H) \leftarrow \text{HEAD}(R)$ 
     $(p_T, \ell_T, r_T) \leftarrow \text{TAIL}(R)$ 
     $q_{Ti} \leftarrow \text{INNERINTERSECTION}(p_T, p_i)$ 
     $q_{iH} \leftarrow \text{INNERINTERSECTION}(p_i, p_H)$ 
    if  $q_{iH} \in \text{LEFTARC}(p_H, \ell_H) \wedge q_{Ti} \in \text{RIGHTARC}(p_T, r_T)$  then
      continue // skip this iteration
    while  $q_{iH} \in \text{RIGHTARC}(p_H, r_H)$  do
       $R \leftarrow \text{REMOVEHEAD}(R)$ 
       $(p_H, \_ , r_H) \leftarrow \text{HEAD}(R)$ 
       $q_{iH} \leftarrow \text{INNERINTERSECTION}(p_i, p_H)$ 
    while  $q_{Ti} \in \text{LEFTARC}(p_T, \ell_T)$  do
       $R \leftarrow \text{REMOVETAIL}(R)$ 
       $(p_T, \ell_T, \_ ) \leftarrow \text{TAIL}(R)$ 
       $q_{Ti} \leftarrow \text{INNERINTERSECTION}(p_T, p_i)$ 
     $R \leftarrow \text{UPDATEHEAD}(R, \text{ARC}(p_H, q_{iH}, r_H))$ 
     $R \leftarrow \text{UPDATETAIL}(R, \text{ARC}(p_T, \ell_T, q_{Ti}))$ 
     $R \leftarrow \text{APPENDTAIL}(R, \text{ARC}(p_i, q_{Ti}, q_{iH}))$ 
  return  $R$ 

```

Algorithm 1 uses the following subroutines. Subroutine $\text{PARABOLA}(f, e)$ creates a representation of a parabola with f as its focus and a line extension of edge e as its directrix. Subroutine $\text{INNERINTERSECTION}(p_i, p_j)$ computes the intersection point q_{ij} of parabola p_i and p_j ; we recall that from Lemma 2, there are two intersection points and this subroutine returns the “inner” one, i.e., q_{ij} , not q_{ji} .

Since our goal is to find a safe region,

$$R = \bigcap_{i=1}^n H(p_i),$$

Algorithm 1 iterates over parabolas p_i producing a partial solution R_i such that:

$$R_i = \bigcap_{j=1}^i H(p_j),$$

i.e., R_i is the safe region for the first i parabolas. We maintain R_i as a cyclic list of parabola arcs:

$$a_1, a_2, \dots, a_k,$$

where each arc a_j is a 3-tuple (p, ℓ, r) which keeps a reference to the parabola $a_j.p$, its left endpoint $a_j.\ell$, and its right endpoint $a_j.r$. We note that with this representation, $a_j.r = a_{j+1}.\ell$ for $1 \leq j < k$, and $a_k.r = a_1.\ell$. We also note that, using the notation defined in Section 2.2, $a_j.r$ is $q_{j(j+1)}$ and $a_j.\ell$ is $q_{(j-1)j}$.

Initially, we start with $R_2 = H(p_1) \cap H(p_2)$. We encode the partial safe region as an ordered list of arcs, $A(R_2) = [a_1, a_2]$, where:

$$\begin{aligned} a_1 &= (p_1, q_{21}, q_{12}) \\ a_2 &= (p_2, q_{12}, q_{21}) \end{aligned}$$

For each iteration $i > 2$, we consider adding $H(p_i)$ to R_{i-1} to produce $R_i = R_{i-1} \cap H(p_i)$. There are three cases:

- *Case 1:* p_i does not change the region, i.e., $R_{i-1} \cap H(p_i) = R_{i-1}$ and we can discard p_i ;
- *Case 2:* p_i clips the region, i.e., all parabola arcs in R_{i-1} remain on the boundary of $R_{i-1} \cap H(p_i)$; or
- *Case 3:* p_i eclipses other parabolas in the region, i.e., some parabola arc is entirely outside $R_{i-1} \cap H(p_i)$.

Figure 6 illustrates these three cases. The safe regions R_{i-1} are shown with additional parabolas p_i with e_i as their directrices.

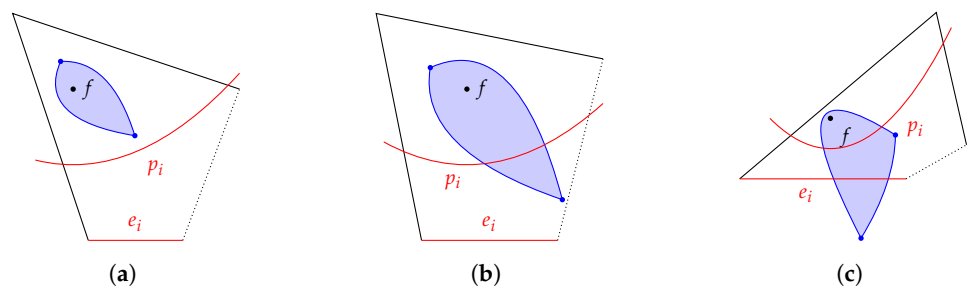


Figure 6. Three cases of adding parabola p_i to the partial safe region R_{i-1} . (a) *Case 1:* p_i does not change the region. (b) *Case 2:* p_i clips the region. (c) *Case 3:* p_i eclipses some parabola.

To distinguish between these cases, our basic procedure is to test if a point lies in $H(p_i)$. The counterclockwise ordering of parabolas ensures that p_i would affect two sequences of arcs, i.e., clockwise,

$$a_k, a_{k-1}, a_{k-2}, \dots,$$

to be referred to as the *neighbors to the left* of p_i , and counterclockwise,

$$a_1, a_2, a_3, \dots,$$

to be referred to as the *neighbors to the right* of p_i ,

We first consider point $q_{k1} = a_k.r$ (which is also $a_1.l$). Lemma 4 below ensures that we are in Case 1 if $q_{k1} \in H(p_i)$. See Figure 7.

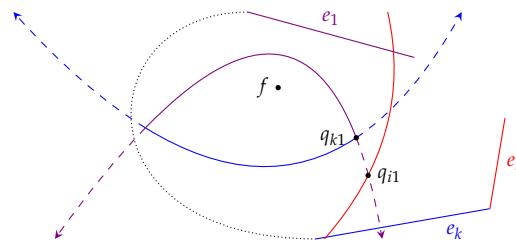


Figure 7. Proof of Lemma 4.

Otherwise, some part of R_{i-1} is below parabola p_i . We in turns consider the points:

$$a_{k-1}.r, a_{k-2}.r, \dots,$$

from the neighbors to the left of p_i and find the largest index j such that $a_j \cap H(p_i) \neq \emptyset$. In this case, the parabolas $a_k.p, a_{k-1}.p, \dots, a_{j+1}.p$ are eclipsed by p_i .

We also process the neighbors to the right of p_i similarly by finding the smallest index j' such that $a_{j'} \cap H(p_i) \neq \emptyset$ together with the sequence of eclipsed arcs $a_1, a_2, \dots, a_{j'-1}$. We note that it can be the case that $j = j'$ when only one arc survives p_i eclipsing.

To construct R_i , we discard eclipsed arcs, add a new arc a_i for p_i , and compute the following:

- The left intersection point $a_i.l = a_j.r$, which is the intersection between p_i and $a_j.p$;
- The right intersection point $a_i.r = a_{j'}.l$, which is the intersection between p_i and $a_{j'}.p$.

Finally, we re-index the arcs in R_i . We quickly remark that this procedure can be seen as a “twin-headed” Graham scan.

The following lemmas show that this procedure is correct.

Lemma 4. *If $q_{k1} \in H(p_i)$, then $R_{i-1} \subseteq H(p_i)$ and $R_i = R_{i-1}$.*

Proof. Since $R_{i-1} \subseteq H(p_1) \cap H(p_k)$, our goal is to show that $H(p_1) \cap H(p_k) \subseteq H(p_i)$ in this case.

Consider the intersection of p_1 and p_k . Recall that the two intersection points q_{k1} and q_{1k} partition both parabolas into their left arcs, central arcs, and right arcs. Let us call them a_k^l, a_k^c, a_k^r and a_1^l, a_1^c, a_1^r .

We now consider the intersection of p_1 and p_i . We show that q_{i1} , the intersection point of p_i and p_1 , is on the left arc a_1^l of p_1 . To see this, we start by rotating the plane such that p_i is in the upright form. Then, we find a region $r = H(p_1) \cap H(p_i)$. Since $q_{k1} \in p_1$ and also $q_{k1} \in H(p_i)$, q_{k1} is on the boundary of $H(p_1) \cap H(p_i) = r$. Again, since $q_{k1} \in p_1$ and also on the boundary of r , traversing from q_{k1} on the boundary of r clockwise with respect to f would reach q_{i1} , by definition of q_{i1} , as claimed.

Using the same argument, we can show that q_{ki} is in the right arc a_k^r of p_k .

Using q_{i1} and q_{ki} , we partition p_i into three arcs— a_1, a_2 , and a_3 —so that a_1 is an unbounded curve with q_{i1} as its end point, a_2 is a bounded part with q_{i1} and q_{ki} as their end points, and finally, a_3 is an unbounded curve with q_{ki} as its end point (see Figure 7).

Using the structure from Lemma 2, we know that $a_1 \cup a_2$ intersects p_k at only $q_{ki} \in a_k^r$. Thus, p_i does not intersect $a_k^c \cup a_k^l$.

Additionally, we know that $a_2 \cup a_3$ intersects p_1 at only $q_{i1} \in a_1^l$, implying that p_i does not intersect $a_1^r \cup a_1^c$.

We can conclude that p_i does not intersect with R_{i-1} because R_{i-1} lies between the unbounded curves $a_k^c \cup a_k^l$ and $a_1^r \cup a_1^c$. \square

We also have a simple contraposition.

Corollary 1. *If $R_{i-1} \not\subseteq H(p_i)$, then $q_{k1} \notin H(p_i)$.*

Let $\hat{R} = \bigcap_{j=1}^i H(p_j)$ be the correctly updated solution, we would like to show that R_i constructed above equals \hat{R} . We remark that the i -th parabola p_i corresponds to edge e_i that comes counterclockwisely after all other edges that contribute to R_{i-1} .

Lemma 5. *If $R_{i-1} \not\subseteq H(p_i)$, the arcs on R_{i-1} 's boundary which do not belong to \hat{R} form a consecutive sequence:*

$$a_j, a_{j+1}, \dots, a_k, a_1, a_2, \dots, a_j.$$

Proof. Lemma 3 ensures that if p_i intersects the boundary of R_{i-1} , p_i touches at most one arc of \hat{R} , the result of the intersection of $H(p_i)$ and R_{i-1} . This implies that the arcs of R_{i-1} do not belong to form a (circular) consecutive sequence. To see this, assume otherwise and note that in that case, p_i would touch more than one arc of \hat{R} .

Our procedure finds the consecutive sequence starting at q_{k1} , the intersection of p_k and p_1 , then iterates through other consecutive points. Thus, the procedure is correct if the starting point is correct, i.e., we start at some intersection point outside \hat{R} . This is indeed the case because Corollary 1 guarantees that when $R_{i-1} \not\subseteq H(p_i)$, q_{k1} is outside \hat{R} . \square

We conclude with our main correctness theorem.

Theorem 1. *Our updating procedure is correct, i.e., $R_{i+1} = \hat{R}$, and the algorithm computes the safe region in linear time.*

Proof. Regarding the updating procedure, we deal with three possible cases. Lemma 4 ensures that our condition for Case 1 is correct. In other cases, Lemma 5 shows that the procedure for deleting arcs is correct. By induction on n , the algorithm thus produces the required safe region.

To analyze the running time, we first note that, except the two inner while loops, for each i , the algorithm runs in $O(1)$ time. To account for the running time of the inner while loops, observe that each iteration of the loop removes one parabola from the list. Since at most n parabolas are inserted in the list, the deletion can take place at most n times, implying the total running time of $O(n)$ for the loops. \square

4. The Number of Arcs of the Safe Region

In this section, we consider the complexity of the boundary of the safe region; in other words, we count the exact number of arcs of the safe region. From previous sections, we derive that a side of the safe region is a parabolic arc with point f as its focus. We also see that some edge of P may not contribute to the resulting safe region, i.e., a parabola associated with it does not touch the safe region. It is natural to ask for the number of arcs of the safe region.

Assuming that the polygon P is fixed, the number of arcs of the safe region depends on the focus f . We denote explicitly by R_f a safe region with point f as its focus. As in [4], this section analyzes the number of arcs of safe region R_f , i.e., $|A(R_f)|$, where $A(R_f)$ is the set of arcs of R_f . Figure 8a shows two safe regions R_{f_2} with query point f_2 and R_{f_3} with query point f_3 .

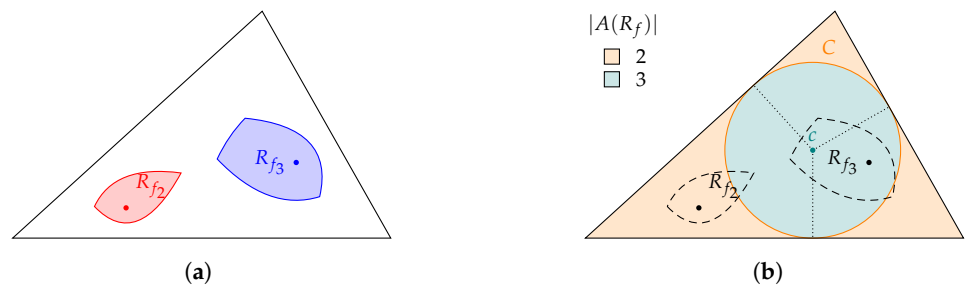


Figure 8. Safe regions with 2 and 3 parabola arcs. (a) Safe regions with query points f_2 and f_3 ; (b) An event circle determines the numbers of arcs.

Akitaya et al. [4] consider the same problem for the case where each side of P is folded onto a line. They show that the straight skeleton of P plays an important role in determining the number of sides of the resulting region. This is true for our case as well. As an example, Figure 8b shows an inscribed circle C which can be determined using the straight skeleton and two safe regions shown previously. We remark that $f_2 \notin C$ but $f_3 \in C$.

We start by defining useful notations related to straight skeletons and event circles. A *straight skeleton* [16] of a polygon P , denoted by $S(P)$, is a subset of P such that for each point $u \in S(P)$, there exist at least two points on δP with the same distance to u . More intuitively, we may see the skeleton as a Voronoi diagram of line segments where each site is an edge of the polygon. The straight skeleton $S(P)$ partitions P into regions, referred to as *faces*. Thus, under the Voronoi interpretation, each face is bounded by exactly one polygon edge as other edges of $S(P)$. We refer to a face that is bounded by polygon edge e_i as face F_i . We also note that a face is also a convex polygon. See Figure 9 for an illustration.

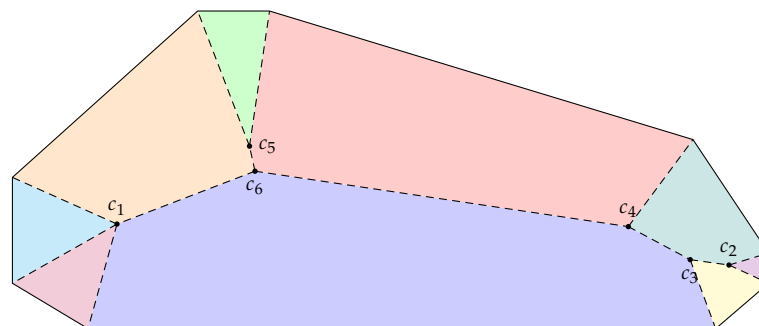


Figure 9. The straight skeleton of polygon P , with each face colored differently. Points c_1, \dots, c_6 are event points.

The skeleton may be viewed as a tree, where each non-leaf node ensures at least three equidistant points on δP . A non-leaf node of $S(P)$ is referred to as an *event point*. A circle centered at an event point and tangential to the nearest edge of the polygon is called an *event circle* of $S(P)$. Let \mathcal{C} be the set of all event circles of $S(P)$, and let $\mathcal{C}_e \subseteq \mathcal{C}$ be a set of event circles tangential to edge e . We also denote by $\text{int}(C)$ an interior of circle C , i.e., the set $\{(x, y) : (x - x_0)^2 + (y - y_0)^2 < r^2\}$ for a circle with center (x_0, y_0) and radius r .

The goal of this section is to show that, under the fixed polygon P , the structure of $A(R_f)$ is governed by event circles of straight skeleton $S(P)$ of P .

We start by analyzing the case when the safe region intersects with the skeleton faces. The following lemma directly follows from the Voronoi interpretation of the straight skeleton.

Lemma 6. For each event circle C with event point c , c is adjacent to face F_i if and only if its corresponding polygon edge e_i is tangential to C .

The following two lemmas provide basic properties for our main theorem in this section.

Lemma 7. For a particular focus f , $\text{int}(R_f)$ intersects with skeleton face F_i adjacent to edge e_i iff the associated parabola p_i is part of the arcs of R_f .

Proof. (\Rightarrow) Assume that $\text{int}(R_f)$ intersects F_i . Since F_i is bounded by a polygon edge and R_f is contained in P , we know that there are parts of the boundary of R_f that intersect F_i . Consider any point u on the boundary of R_f inside F_i . Clearly, u must be on an arc of some parabola, i.e., we have that:

$$\min_j |\overline{uu_j}| = |\overline{uf}|,$$

where u_j is an orthogonal projection of u onto e_j . Since all points in F_i are closer to e_i than other edges, the minimizer of the above term is u_i ; thus, u must also lie on p_i , i.e., p_i is part of arcs of R_f .

(\Leftarrow) We prove by contradiction. Assume that $\text{int}(R_f)$ does not intersect F_i , but p_i is part of the boundary of R_f . Consider any point $u \in p_i$ on the boundary. Since $\text{int}(R_f)$ is disjoint from F_i , u is strictly in some face F_j . In this case, we have that:

$$|\overline{uf}| = |\overline{uu_i}| > |\overline{uu_j}|,$$

where u_i and u_j are orthogonal projections of u onto e_i and e_j , implying that $u \notin H(p_j)$, a contradiction. \square

Lemma 8. For $C \in \mathcal{C}$ with event point c , a safe region R_f strictly contains an event point c , i.e., $c \in \text{int}(R_f)$, iff $f \in \text{int}(C)$.

Proof. Let r be the radius of an event circle C . Project c orthogonally to a line extension of every edge e_i , named the projected point c_i .

(\Leftarrow) Assume that $f \in \text{int}(C)$, i.e., $|\overline{cf}| < r$. We show that $r \in H(p_i)$ for every parabola p_i associated with polygon edge e_i . This is the case when r is strictly closer to f than every other edge e_i . Consider each edge e_i tangent to C , we have $|\overline{cf}| < r = |\overline{cc_i}|$. For edge e_i not tangent to C , we have that $|\overline{cc_i}| > r$; thus, $|\overline{cf}| < r < |\overline{cc_i}|$. Hence, c is in the safe region R_f .

(\Rightarrow) Assume that $f \notin \text{int}(C)$. In this case, we have $|\overline{cf}| \geq r$. Since C is an event circle, there exists edge e_i tangent to C . For that particular edge, we have $|\overline{cc_i}| = r$. Thus, $|\overline{cf}| \geq r = |\overline{cc_i}|$, and c is not strictly contained in the safe region R_f . \square

The following theorem gives the number of boundary arcs of R_f as a function of event circles containing f .

Theorem 2. If f is strictly inside some event circle, i.e., $f \in \text{int}(C)$ for some $C \in \mathcal{C}$, then:

$$|A(R_f)| = |\{e_i \in E(P) : \text{there exists } C \in \mathcal{C}_{e_i} \text{ s.t. } f \in \text{int}(C)\}|$$

Otherwise, $|A(R_f)| = 2$.

Proof. We first assume that $f \in \text{int}(C)$ for some event circle C . Consider each event circle C with event point c such that $f \in \text{int}(C)$. From Lemma 8, we know that $c \in \text{int}(R_f)$. This also means that $\text{int}(R_f)$ intersects every face F_i adjacent to event point c . Lemma 6 ensures that these faces F_i 's correspond with edges e_i 's tangent to C , the set of edges e_i such that $C \in \mathcal{C}_{e_i}$. Since Lemma 7 ensures that for each face F_i adjacent to edge e_i intersecting with R_f , the parabola p_i appears as an arc of R_f , we have that for each tangent edge e_i of C , its parabola p_i appears as an arc in R_f . The lemma, in this case, follows by taking the union of all boundary edges from every event circle $C \in \mathcal{C}$ that f is strictly inside.

On the other hand, if f is not strictly contained in any event circle $C \in \mathcal{C}$, Lemma 2 ensures that the safe region must touch two parabolas. \square

Figure 10 shows an application of Theorem 2. The event circles are shown with their intersections. From Theorem 2, for each point f , the number of arcs of $A(R_f)$ depends

on the number of edges tangent to event circles containing f . Thus, every point f in a particular intersection of event circles has the same value of $|A(R_f)|$. Each intersection in Figure 10 is shown with a different color depending on the value of $|A(R_f)|$ for a query point f inside it. Remark again that for query point f in the area outside any event circles, the value of $|A(R_f)|$ is 2.

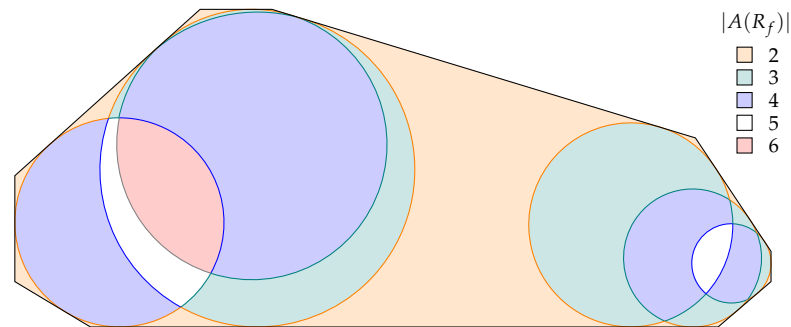


Figure 10. Intersections of event circles from the straight skeleton determine $|A(R_f)|$.

Alternatively, one may view Theorem 2 with the conic section interpretation as follows. The input polygon P induces n cutting planes, forming the straight skeleton and their corresponding faces when projected onto the xy -plane, and the point f is represented as a cone whose apex is at f .

The structural results in this section give another linear-time algorithm for finding safe regions, by first finding straight skeleton in $O(n)$ -time using [17], then computing event circles, and finally using this information to find the set of edges contributing to the arcs of the safe region. However, we believe that the results in this section contribute mainly to the structural understanding of the problem and may serve as a guideline for tackling harder problems, especially the non-convex case of the problem. We discuss this in Section 5.1.

5. Conclusions and Open Problems

We present a linear-time algorithm for finding a safe region for folding each point on the boundary of a convex polygon P to point $f \in P$. We also give structural properties related to the number of arcs in a safe region for each focal point f , based on straight skeletons. We note the crucial roles of straight skeletons in our problem as well as other problems in origami design, as can be seen in [18]. An interesting direction for future work is to investigate problems with the similar structures while using straight skeletons as keys.

As mentioned in the introduction, we also hope that our results show interesting connections between the two problems posted by Akitaya et al. [4].

5.1. Remarks on Non-Convex Polygons

Results in Section 4 shed some light on non-convex cases. However, there are issues with the current approach. When dealing with non-convex polygons, there are two related concepts: straight skeletons [16] and medial axes [19] (see also [17,20]). For a given polygon, a medial axis contains points with equal distance to more than one points on δP , while a straight skeleton is a Voronoi diagram where each site is a *line extension* of each edge. They are the same in convex polygons, however, in non-convex polygons, their medial axes contain curved segments.

In our application, since we can only fold every point on each polygon edge, but not points on the line extension of the edge, it makes sense to consider a medial axis. However, each face in the medial axis can be bounded by more than one polygon edges, breaking down one of our key assumptions. We leave the investigation of this approach to non-convex polygons as an important open question.

Author Contributions: Conceptualization, N.P. and J.F.; methodology, N.P. and J.F.; formal analysis, N.P. and J.F.; writing—original draft preparation, N.P.; writing—review and editing, J.F. All authors have read and agreed to the published version of the manuscript.

Funding: This research was funded by the Thailand Research Fund grant number RSA-6180074.

Data Availability Statement: No new data were created or analyzed in this study. Data sharing is not applicable to this article.

Acknowledgments: The authors would like to thank organizers and participants of JCDCGGG 2022, especially Hugo Akitaya, for giving feedback on the presentation of this work and pointing out the important aspect. We also thank anonymous reviewers for insightful feedbacks.

Conflicts of Interest: The authors declare no conflict of interest.

References

1. Lang, R.J. Computational Origami: From Flapping Birds to Space Telescopes. In Proceedings of the Proceedings of the Twenty-Fifth Annual Symposium on Computational Geometry (SCG '09), Aarhus, Denmark, 8–10 June 2009; Association for Computing Machinery: New York, NY, USA, 2009; p. 159–162. [\[CrossRef\]](#)
2. Demaine, E.D.; O'Rourke, J. *Geometric Folding Algorithms: Linkages, Origami, Polyhedra*; reprint ed.; Cambridge University Press: New York, NY, USA, 2008.
3. Hull, T.C. *Origametry: Mathematical Methods in Paper Folding*; Cambridge University Press: Cambridge, UK, 2020.
4. Akitaya, H.A.; Ballinger, B.; Demaine, E.D.; Hull, T.C.; Schmidt, C. Folding Points to a Point and Lines to a Line. In Proceedings of the 33rd Canadian Conference on Computational Geometry (CCCG 2021), Halifax, NS, Canada, 10–12 August 2021; Dalhousie University: Halifax, NS, Canada, 2021; pp. 271–278.
5. Akitaya, H.A.; Demaine, E.D.; Ku, J.S. Simple Folding is Really Hard. *J. Inf. Process.* **2017**, *25*, 580–589. [\[CrossRef\]](#)
6. Abel, Z.; Demaine, E.D.; Demaine, M.L.; Eppstein, D.; Lubiw, A.; Uehara, R. Flat foldings of plane graphs with prescribed angles and edge lengths. *J. Comput. Geom.* **2018**, *9*, 74–93. [\[CrossRef\]](#)
7. Dambrogio, J.; Ghassaei, A.; Smith, D.; Jackson, H.; Demaine, M.; Davis, G.; Mills, D.; Ahrendt, R.; Akkerman, N.; van der Linden, D.; et al. Unlocking history through automated virtual unfolding of sealed documents imaged by X-ray microtomography. *Nat. Commun.* **2021**, *12*, 1184. [\[CrossRef\]](#) [\[PubMed\]](#)
8. Felton, S.; Tolley, M.; Demaine, E.; Rus, D.; Wood, R. A method for building self-folding machines. *Science* **2014**, *345*, 644–646. [\[CrossRef\]](#) [\[PubMed\]](#)
9. Hull, T.C. Solving cubics with creases: The work of Beloch and Lill. *Am. Math. Mon.* **2011**, *118*, 307–315. [\[CrossRef\]](#)
10. Haga, K. Proposal of a term origamics for plastic origami-workless scientific origami. In Proceedings of the Second International Meeting of Origami Science and Scientific Origami, Otsu, Japan, 29 November–2 December 1994; ABSTRACT A-3, pp. 29–32.
11. Haga, K. *Origamics: Mathematical Explorations through Paper Folding*; World Scientific: Singapore, 2008.
12. Hull, T. *Project Origami: Activities for Exploring Mathematics*, 2nd ed.; A K Peters: Natick, MA, USA; CRC Press: Boca Raton, FL, USA, 2013.
13. Aurenhammer, F.; Klein, R.; Lee, D.T. *Voronoi Diagrams and Delaunay Triangulations*; World Scientific: Singapore, 2013.
14. Fortune, S. A sweepline algorithm for Voronoi diagrams. In Proceedings of the Second Annual Symposium on Computational Geometry, Yorktown Heights, NY, USA, 2–4 June 1986; pp. 313–322.
15. Graham, R. An efficient algorithm for determining the convex hull of a finite planar set. *Inf. Process. Lett.* **1972**, *1*, 132–133. [\[CrossRef\]](#)
16. Aichholzer, O.; Aurenhammer, F. Straight skeletons for general polygonal figures in the plane. In Proceedings of the Computing and Combinatorics, Hong Kong, China, 17–19 June 1996; Cai, J.Y., Wong, C.K., Eds.; Springer: Berlin/Heidelberg, Germany, 1996; pp. 117–126.
17. Chin, F.; Snoeyink, J.; Wang, C.A. Finding the Medial Axis of a Simple Polygon in Linear Time. *Discret. Comput. Geom.* **1999**, *21*, 405–420. [\[CrossRef\]](#)
18. Lang, R.J. A computational algorithm for origami design. In Proceedings of the Twelfth Annual Symposium on Computational Geometry, Philadelphia, PA, USA, 24–26 May 1996; pp. 98–105.
19. Blum, H. A transformation for extracting new descriptors of shape. In *Models for Perception of Speech and Visual Form*; Wathen-Dunn, W., Ed.; MIT Press: Cambridge, MA, USA, 1967.
20. Attali, D.; Boissonnat, J.D.; Edelsbrunner, H. Stability and Computation of Medial Axes—A State-of-the-Art Report. In *Mathematical Foundations of Scientific Visualization, Computer Graphics, and Massive Data Exploration*; Springer: Berlin/Heidelberg, Germany, 2009; pp. 109–125. [\[CrossRef\]](#)

Disclaimer/Publisher's Note: The statements, opinions and data contained in all publications are solely those of the individual author(s) and contributor(s) and not of MDPI and/or the editor(s). MDPI and/or the editor(s) disclaim responsibility for any injury to people or property resulting from any ideas, methods, instructions or products referred to in the content.